Synthesis and properties of a redox-switchable calix[6]arene-based molecular lasso

Received 00th January 20xx,
Accepted 00th January 20xx

Synthesis and Properties of a Redox-switchable Calix[6]arene-based Molecular Lasso†

Guido Orlandini,[a] Lorenzo Casimiro,[b] Margherita Bazzoni,[a] Beatrice Cogliati,[a] Alberto Credi,[c,d] Marco Lucarini,[b] Serena Silvi,*[b] Arturo Arduini,*[a] and Andrea Secchi*[a]

The synthesis and characterisation of calix[6]arene-based lasso-like molecular structures is described. These interwoven structures consist of an electrochemical responsive *N*,*N*′-dialkylviologen arm covalently anchored at the upper rim of a triphenylureido calix[6]arene-based wheel. Upon reduction of the viologen core, a hollow tridimensional macrocyclic structure can be generated. This process is reversible, and the original lasso-like structure can be regenerated by oxidizing the viologen arm to its original dicationic form. Electrochemical and EPR techniques investigated the ability of the system to perform threading/dethreading movements upon redox switching. The functionalisation of the arm ω-hydroxy ending with a bulky diphenylacetyl group converts the self-threaded structure in a blocked interwoven molecular compound belonging to the class of [1]rotaxanes. The ability to form dimeric structures in the shape of a [*c*2]daisy chain was also demonstrated, an unprecedented result for calixarene macrocycles.

Introduction

The development of molecular systems able to perform, reversibly, mechanical movements under the action of external energy stimuli is a topic of current interdisciplinary interest. In the last decades, one of the most difficult challenges in the field of artificial molecular machines[1–3] was the construction of devices able to mimic the function of relevant biological structures.[4] Among these structures, lasso peptides[5] represent a class of self-entangled natural species characterised by a macrocycle of 7 to 9 amino acid residues threaded by a longer segment of 8 to 15 residues.[6] An isopeptide bond joins the macrocyclic component to the threaded segment. The threading-unthreading behaviour of the linear peptide segment strictly depends on the bulkiness of the side chains present in the amino acid residues of its terminal part. As a consequence, these compounds can be considered as naturally occurring [1](pseudo)rotaxane species.[7,8]

The design and synthesis of synthetic molecular actuators capable of mimicking the behaviour of lasso peptides could, in principle, open the way to a comprehension of their not yet fully disclosed biological role. Several examples of self-complexing (pseudo)rotaxanes[2] based on crown ethers,[9–11] cyclobis(paraquat-*p*-phenylene)s,[12–14] cyclodextrins,[15–17] and pillarenes[18–21] are reported in the literature. Nevertheless, molecular interlocked species belonging to the class of [1]pseudorotaxanes which are capable of switching from a self-threaded to a non-threaded form upon the application of a suitable external stimulus are still rather uncommon.[11,12,16,18] Among them, a straightforward example has been recently published by Stoddart and co-workers,[14] which employed a radical-pairing interaction to reversibly thread and unthread a viologen-based molecular rope inside a cyclobis(paraquat-*p*-phenylene) loop.

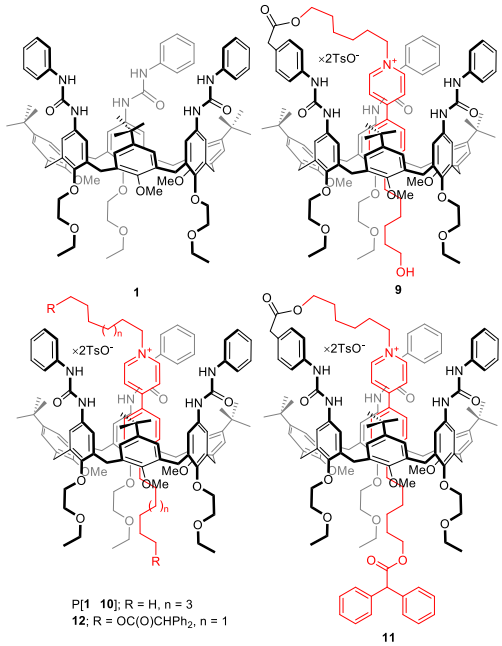

Chart 1 Tris(*N*-phenylureido)calix[6]arene **1**, [2]pseudorotaxane P[**1**⊃**10**], [1]pseudorotaxane **9**, [1]rotaxane **11**, and [2]rotaxane **12**.

[a] *Dipartimento di Scienze Chimiche, della Vita e della Sostenibilità Ambientale, Università di Parma, Parco Area delle Scienze 17/A, I-43124 Parma, Italy.*
[b] *Dipartimento di Chimica "G. Ciamician", Università di Bologna, Via Selmi 2, I-40126, Italy.*
[c] *Istituto per la Sintesi Organica e la Fotoreattività, Consiglio Nazionale delle Ricerche, via Gobetti 101, I-40129 Bologna, Italy.*
[d] *Dipartimento di Chimica Industriale "Toso Montanari", Viale del Risorgimento 4, I-40136, Bologna, Italy*
†Electronic Supplementary Information (ESI) available: NMR, EPR and electrochemical data. See DOI:

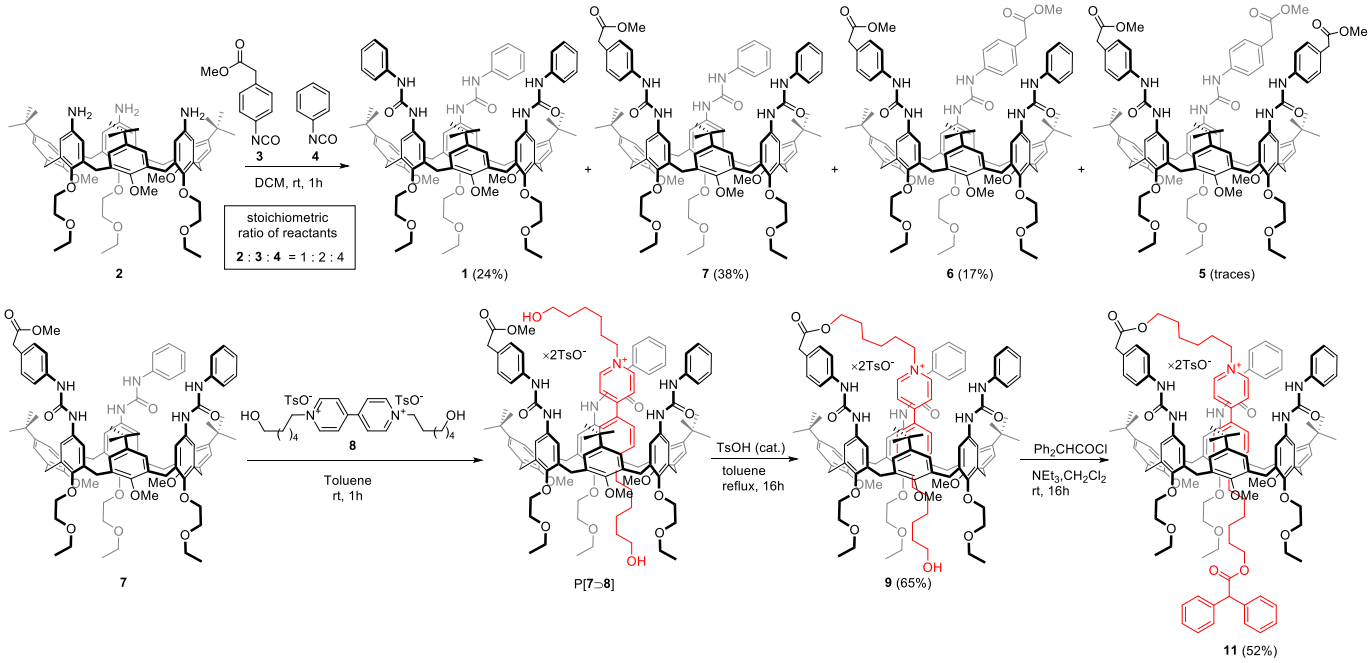

Scheme 1 Synthesis of calix[6]arene-based [1]pseudorotaxane **9** and [1]rotaxane **11**.

Calix[6]arenes are a class of synthetic macrocyclic hosts that have been successfully used as platforms for the construction of working devices and MIMs.[22] In particular, in our group, we have used tris-(*N*-phenylureido) calix[6]arene derivatives, such as **1** (Chart 1), which can give with *N,N'*-dialkyl viologen salts a series of pseudorotaxane complexes or MIMs belonging to the class of rotaxanes and catenanes.[23,24] To date, there are no examples in the literature of [1](pseudo)rotaxane complexes based on calixarene architectures. To expand the scope of these devices, in this paper we present the synthesis and properties of a tris-(*N*-phenylureido) calix[6]arene derivative (**9**) (Chart 1) capable to self-assemble in non-polar solvents to originate self-entangled species belonging to the class of [1](pseudo)rotaxanes.

Results and discussion

Design and synthesis of the calix[6]arene derivatives

The tris-(*N*-phenylureido) calix[6]arene derivative **9** is decorated on one of its three phenylurea moieties at the upper rim with a flexible alkyl arm containing a 4,4'-bipyridinium core and ω-functionalised with a hydroxy group. For its synthesis, we devised the convergent approach described in Scheme 1. Such approach was inspired by the synthesis of similar systems,[25–27] and it is based on the insertion on the macrocyclic upper rim of a methyl ester anchoring group that, in principle, can readily undergo a transesterification process with one of the hydroxy groups of a symmetric *N,N*-(ω-hydroxy)dialkyl viologen-based axle threaded inside the calix[6]arene wheel. To this aim, we first synthesised the calix[6]arene derivative **7** by reacting triamino calix[6]arene (**2**)[28] with mixtures of phenyl isocyanates **3** and **4**. Because of the identical reactivity of the amino groups of **2** towards these isocyanates, this reaction may yield complicated combinations of the four possible calix[6]arene derivatives (**1** and **5**-**7**) depicted in Scheme 1. However, after several attempts carried out by varying the stoichiometric ratio between the reagents, we succeeded in isolating the target monomethylester calix[6]arene **7** in good yields (38%) by reacting **2** with phenyl isocyanates **3** and **4** in 1:2:4 stoichiometric ratio. In these conditions, after chromatographic purification, the other derivatives were separated in traces (**5**) up to appreciable amounts (**1** and **6**) (Scheme 1).

The ^{1}H NMR spectrum of **7** taken in $CDCl_3$ (Figure 1e and Figure S1, ESI) shows the presence of a very broad signal at ca. δ = 2.9 ppm for the methoxy groups (*e*) at the macrocycle lower rim that, being oriented inward the electron-rich cavity, are suffering an extensive shielding anisotropic effect (see Figure 1 for labelling). The two broad signals at δ = 4.4 and 3.5 ppm, for the axial (*g'*) and equatorial (*g*) protons of the bridging methylene units, respectively, are in agreement with a calixarene macrocycle having a large fluxionality on the NMR time-scale.[29]

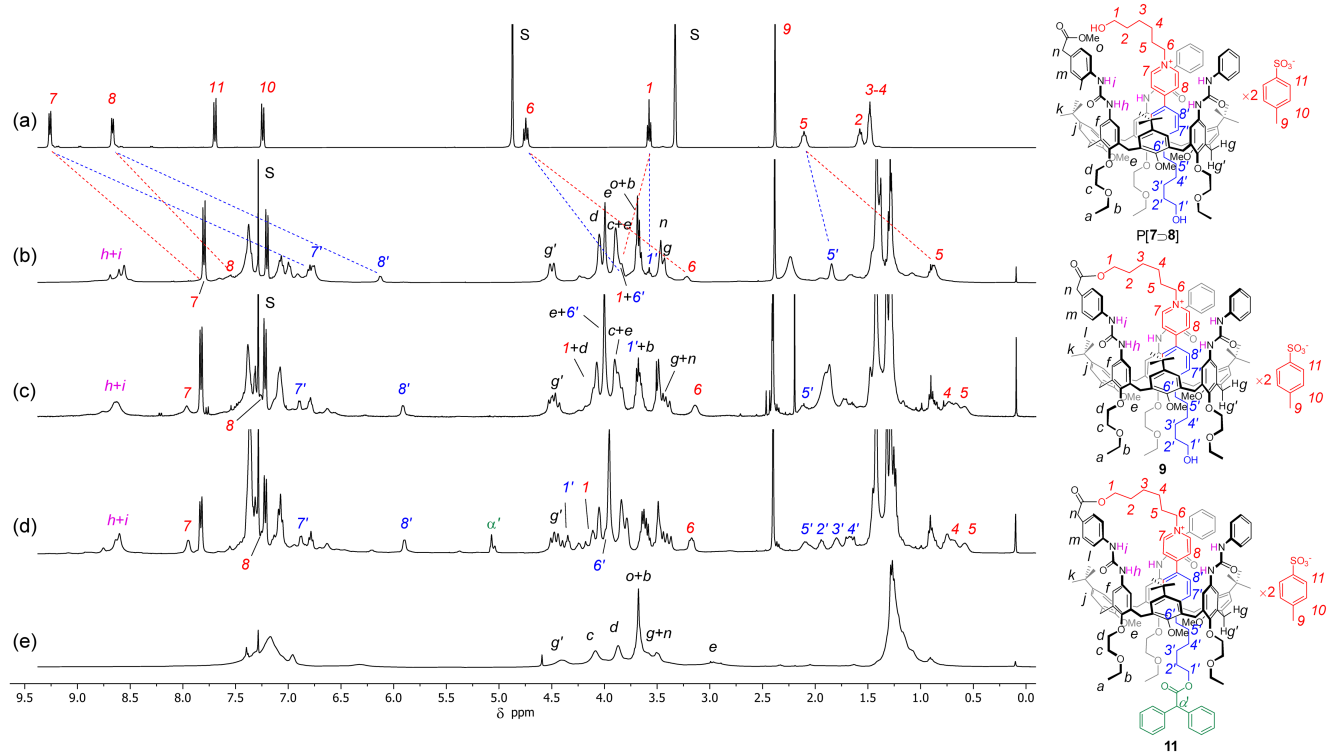

Figure 1 ^{1}H NMR (400 MHz) stack plot of (a) axle **8**, (b) [2]pseudorotaxane P[**7**⊃**8**], (c) [1]pseudorotaxane **9**, (d) [1]rotaxane **11**, and (e) calix[6]arene wheel **7**. For solubility reasons spectrum (a) was taken in CD_3OD, whereas spectra (b-e) in $CDCl_3$. The shift of the most representative resonances is indicated with dashed lines.

The signals relative to the CH_2COOMe anchoring group are not easily recognised in the ^{1}H NMR spectrum because of their extensive overlapping with other macrocycle signals. However, they were identified through the analysis of a 2D HSQC spectrum (Figure S3, ESI) that displays two cross-peaks at δ (F_2,F_1) = 3.50; 40.4 and 3.68; 52.0 ppm, which were assigned to the methylene (*n*) and the carbomethoxy (*o*) protons of the anchoring group, respectively. ESI-MS measurements then finally confirmed the identity of **7** (Figure S4, ESI).

The preparation of calix[6]arene **9** required an accurate design: *i*) the formation of a highly stable pseudorotaxane complex between **7** and a viologen axle endowed with two ω-hydroxyalkyl chains of proper length, followed by *ii*) a transesterification reaction between the carbomethoxy unit present on the upper rim of the wheel and one of the axle OH groups. The choice to use **8** as axle (Scheme 1), which is characterised by two C6OH alkyl chains, was prompted by molecular mechanics calculations (MMFF94 force field) carried out on the structure of the corresponding pseudorotaxanes P[**7**⊃**8**] (Figure 2a). These calculations evidenced that, upon threading, axle **8** has the proper length to orient one of its terminal OH groups close to the carbomethoxy unit at the macrocycle upper rim, favouring the transesterification reaction. On the other hand, the opposite C6OH alkyl chain, protruding from the lower rim of the macrocycle, becomes amenable for a possible stoppering reaction that can block the resulting interwoven structure in a lasso form (Figure 2b).

The synthesis of **9** was indeed accomplished with the two-step procedure described in Scheme 1. In the first step, a heterogeneous 1:1 mixture of **7** and **8**[30] was stirred at room temperature in toluene to yield, after a fast self-assembly process, the pseudorotaxane P[**7**⊃**8**]. The formation of the interwoven species was witnessed by the intense red colour assumed by the now homogeneous solution, typical of these charge-transfer complexes.[31] The ^{1}H NMR spectrum of P[**7**⊃**8**] in $CDCl_3$ (Figure 1b) shows the usual pattern of signals of this type of pseudorotaxane complexes.[29–33] In particular, the flattened *cone* conformation adopted on the NMR time-scale by the threaded macrocycle is verified by the presence of two doublets at δ = 3.5 and 4.5 ppm, due to the geminal coupling between the axial (*g'*) and equatorial (*g*) protons of the calix[6]arene bridging methylene groups.

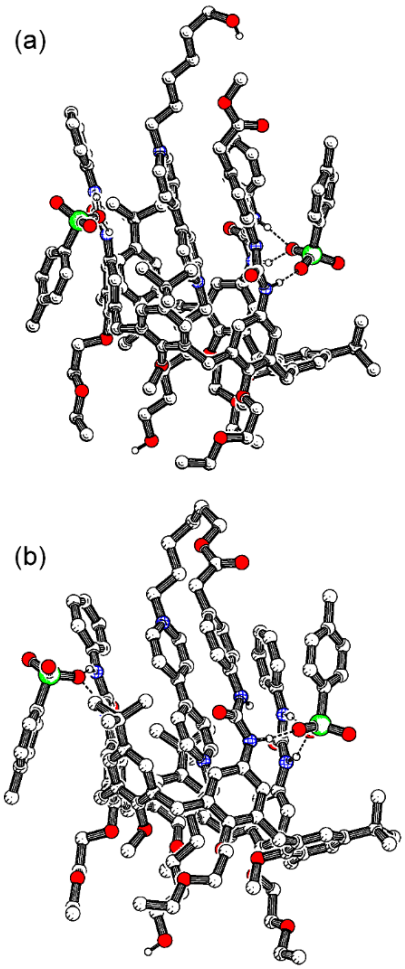

Figure 2 Pluton representation of the minimised structures for (a) [2]pseudorotaxane P[**7**⊃**8**], and (b) [1]pseudorotaxane **9**, according to the MMFF94 force field. Hydrogen atoms except those on heteroatoms have been omitted for clarity.

The inclusion of the axle inside the wheel was inferred by the significant up-field shifts (up to 2.6 ppm) endured by the resonances of the aromatic protons of the bis-pyridinium core (*7*, *7'*, *8* and *8'*) and by those of the adjacent *N*-CH_2- protons (*6* and *6'*) (*cf.* Figure 1a and 1b, dashed lines). The downfield shift of the signals relative to the methoxy groups (*e*), from 2.9 to 3.9 ppm, and of the urea NH protons (*h* and *i*) are also in agreement with a rigidified threaded calix[6]arene structure (see also Figures S5-7, ESI).[29,32,33]

In the following step, the transesterification reaction to give **9** was accomplished by adding a catalytic amount of *p*-toluenesulfonic acid to a refluxing toluene solution of P[**7**⊃**8**]. The transesterification reaction went to completion after refluxing 16h, and the desired self-threaded [1]pseudorotaxane **9** was isolated in 65% yield after chromatographic separation. This compound was fully characterised using NMR and MS measurements (Figures S8-12, ESI). Its ^{1}H NMR spectrum taken in $CDCl_3$ (Figure 1c) presents an overall similarity with that of its pseudorotaxane precursor (*cf.* Figures 1b and 1c) witnessing that, in this weakly polar solvent, the alkyl pyridinium arm is still threaded inside the aromatic cavity. The linkage between the wheel and the thread was confirmed by *i*) the disappearance in the spectrum of **9** of the signal relative to the methyl ester group (*o*), previously visible as a singlet at δ~3.7 ppm (Figure 1b), and *ii*) the downfield shift (from 3.6 to 4.2 ppm) of the resonance relative to the axle terminal methylene group (*1*). The inherent asymmetry of this new linked compound, together with the restricted mobility of the thread, induces a change of multiplicity of the signals relative to the bridging methylene protons (*g* and *g'*) of the macrocycle. The identification of the above resonances was accomplished through the comparison of the corresponding 2D HSQC spectra (Figure S11, ESI). The presence of a doubly charged base peak at m/z = 932.1 in the ESI-MS spectrum (Figure S12, ESI) confirmed the identity of **9**.

The self-complementary structure of **9** could also generate dimeric supramolecular complexes with the shape of [*c*2]daisy chain. Inspired by the work of Strutt et al.[27] on similar systems, a series of diffusion-ordered spectroscopy (DOSY) experiments[34,35] were carried out in C_6D_6 to verify the ability of **9** to give rise to mechanically interlinked dimers having a [*c*2]daisy chain architecture. The DOSY experiments were performed on four solutions at increasing concentration of **9** (7, 12, 22 and 30 mM), and the linear fitting of the attenuation profile (see the Experimental Section) of the NMR spectrum resonances yielded in each experiment a diffusion coefficient *D* reflecting the aggregation state of the species diffusing in solution. For reference, the same series of DOSY experiments was also carried out on pseudorotaxane P[**1**⊃**10**][31] (see Chart 1 and Figure 3) that, differently from **9**, cannot dimerize since its axle, the *N*,*N*-dioctyl viologen ditosylate (**10**), is not covalently linked to the calix[6]arene macrocycle. The experiment carried out at the lower concentration (7 mM) yielded very similar diffusion coefficients for both **9** (D = 3.07×10^{-6} cm^{2}s^{-1}) and P[**1**⊃**10**] (D = 2.99×10^{-6} cm^{2}s^{-1}) (see red and green contours of Figure 3). These results suggest that, at this concentration, **9** likely assumes a [*c*1]daisy chain structure. In this architecture, the alkylviologen unit appended to the upper rim of the macrocycle is self-threaded (intramolecular threading) in the electron-rich calixarene cavity (see Figures 2b and 3). A significant lowering of the diffusion coefficient (D = 2.51×10^{-6} cm^2 s^{-1}) for **9** was instead observed starting from the experiment accomplished on the 22 mM solution. The value of *D* remained almost unaffected even at a higher concentration (30 mM) of the solution of **9** (see also Figures S18-21, ESI). A good estimate of the molecular weight of the species diffusing in a solution can be determined by applying a relationship derived from the Stokes-Einstein equation for spherical species:[35]

$$MW(\mathbf{9}) = [D(\mathrm{P}[\mathbf{1}\supset\mathbf{10}])/D(\mathbf{9})]^3 \times MW(\mathrm{P}[\mathbf{1}\supset\mathbf{10}])$$

where MW(**9**) is the molecular weight of the assembled species deriving from **9** that are diffusing in solution, D(P[**1**⊃**10**]) and D(**9**) are the measured diffusion coefficients, and MW(P[**1**⊃**10**]) is the molecular weight of the pseudorotaxane taken as the reference. For the 22 mM solution, we calculated a molecular weight of 4009 D. Such value is almost twice the molecular weight of the self-threaded form of **9** (2207 D), thus suggesting that, at this concentration, a threaded [*c*2]daisy chain structure is the prevalent species present in solution (see Figure 3).‡

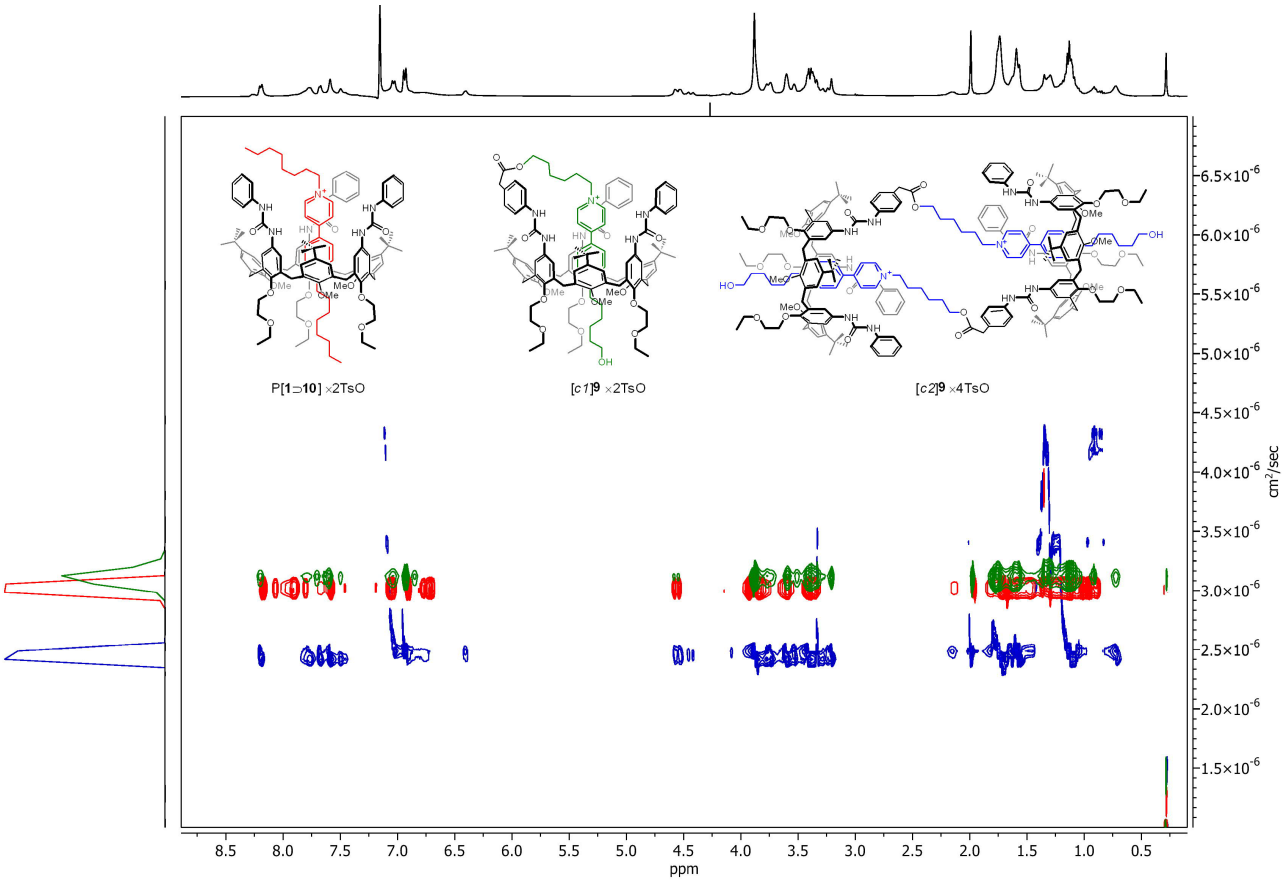

Figure 3 Superimposed DOSY (400 MHz) spectra of a 7 mM (green contours, D = 3.07×10^{-6} cm^{2}s^{-1}), 22 mM (blue contours, D = 2.51×10^{-6} cm^{2}s^{-1}) solution of **9**, and of a 22 mM (red contours, D = 2.99×10^{-6} cm^{2}s^{-1}) solution of P[**1**⊃**10**] in C_6D_6. The F_2 projection is relative to a 22 mM solution of **9**.

It was then envisaged that carrying out a stoppering reaction with diphenylacetyl chloride on the OH terminus of **9** (Scheme 1) at a concentration of 22 mM or higher could block this self-entangled structure in a [*c*2]daisy chain rotaxane. A red solid product was isolated from the reaction mixture in 52% of yield and characterised by NMR and MS measurements (Figures S13-17, ESI). These analyses confirmed that the axle stoppering reaction was successful. In particular, with respect to its precursor, the ^{1}H NMR spectrum of the stoppered compound, taken in $CDCl_3$ solution (Figure 1d), shows a downfield shift (+0.7 ppm) of the resonance relative to the protons of the methylene group (*1′*), and the presence of a singlet at δ = 5.07 ppm, which, based on our previous works,[29,30] was assigned to the resonance of the diphenylacetyl ester methine proton (α'). The other main features of the spectrum resemble those of its precursor except for the aromatic region of the spectrum in which further signals are present due to the presence of the aromatic protons of the diphenylacetyl stopper. The HR-MS measurements revealed the presence in the spectrum (Figure S17, ESI) of a doubly charged base peak at m/z = 1029.06775 D, which is in good agreement with the predicted mass of a stoppered self-threaded [1]rotaxane (**11**) (Scheme 1). These results thus showed us that the stoppering reaction of the OH termini occurs preferentially on the self-complexed [1]pseudorotaxane **9** rather than on the doubly threaded [*c*2]daisy chain structure, driving a re-equilibration between the dimeric and monomeric structures.

Optical and electrochemical measurements

UV- VIS absorption spectra of **9** and **11** were recorded in CH_2Cl_2 and CH_3CN, at concentrations ca. 2×10^{-4} M. The spectra are similar in both solvents, as observed in related rotaxane and pseudorotaxane systems,[30,31] and are characterized by a strong absorption in the UV, with an absorption coefficient close to 10^5 M^{-1} cm^{-1}, and a broad and weak band around 460 nm, with an absorption coefficient around 500 M^{-1} cm^{-1} (Figure 4).

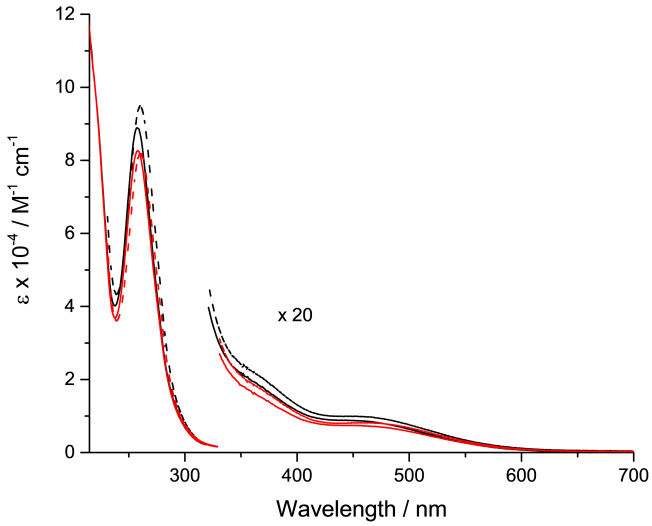

Figure 4 Absorption spectra of **11** (red) and **9** (black) in CH_3CN (solid line) and CH_2Cl_2 (dashed line).

The spectral features are consistent with the presence of a bipyridinium unit engulfed inside the cavity of the calixarene. In particular, the lower energy band is ascribed to the presence of charge-transfer interactions between the electron-accepting bipyridinium moiety and the electron-donating cavity of the macrocycle.[31] The similarity of the spectra of **9** in the two solvents suggests high stability for the inclusion complex, regardless of the solvent.[31]

The electrochemical investigations were performed using cyclic voltammetry (CV) and differential pulse voltammetry (DPV) on CH_2Cl_2 and CH_3CN solutions of **9** and **11**, at concentrations around 2×10^{-4} M. The results of the electrochemical experiments are reported in Table 1 and Figure 5. As a model compound of the free bipyridinium moiety, which is the electroactive unit, electrochemical experiments were also performed on the ditosylate salt of 1,1'-dioctyl-4,4'-bipyridinium (**10**). The bipyridinium moiety is generally characterised by two monoelectronic reversible reduction processes. These two processes are affected by encapsulation inside the cavity of the calixarene, on account of the charge transfer interaction between the electron acceptor bipyridinium unit and the electron donor ring scaffold.[30,31] The [1]rotaxane **11** displays the typical electrochemical behaviour of related [2]rotaxanes:[30,36,37] both reduction waves of the bipyridinium moiety are shifted to more negative values (Table 1), regardless of the solvent.[30,37] The bipyridinium unit is more difficult to reduce because it is engaged in electron donor-acceptor interactions with the calixarene.

The electrochemical features of **9** are different with respect to **11**, because the bipyridinium unit can dethread from the macrocycle, and they are also solvent dependent. In CH_3CN (Figure 5, left), the first reduction wave is quasi-reversible and is about 200 mV more negative than in the corresponding free axle in solution.[38] Conversely, the second reduction process is close to the one of the free bipyridinium unit in solution. A small wave, however, is still present at -1.2 V, which can be ascribed to the encapsulated axle[30,37] (marked with an asterisk in Figure 5). In CH_2Cl_2 (Figure 5, right), the situation is qualitatively similar: two quasi-reversible voltammetric waves are observed, related to the two reduction processes of the bipyridinium unit. The potential of the first process is shifted negatively with respect to axle **10**, and comparable with that of [1]rotaxane **11**, whereas the second reduction occurs at a significantly less negative potential than in **11**.

In both solvents, the shift of the first reduction process to more negative potential values with respect to **10** and its resemblance with the same process in **11** (Figure 5, red line) confirms that the electroactive unit is encapsulated in the cavity of the calixarene and engaged in charge-transfer interactions. As expected, these interactions are weakened upon reduction, causing the dethreading of the axle from the wheel.[31] Such an interpretation is supported by the similarity of the second reduction potential of **9** with that of **10** (Figure 5, blue line). If the bipyridinium radical cation remained inside the calixarene host, its reduction to the neutral form would have occurred at the same potential observed in **11**, where encapsulation is enforced by a mechanical bond. EPR measurements are fully consistent with this scenario (*vide infra*). The reversibility of these switching processes is confirmed by the chemical reversibility of the CV patterns.

A closer analysis of the electrochemical behaviour of **9**, however, reveals significant differences between the investigated solvents from a quantitative viewpoint. While in CH_3CN the shape of the voltammograms is not largely affected by the scan rate in the investigated range, in CH_2Cl_2 the cathodic and anodic peaks of the first reduction wave are always separated by more than 100 mV and become more separated as the scan rate is increased (Figure S27, ESI). In fact, the first cathodic peak is almost superimposed to the second reduction process (Figure 5, right) at a potential value close to the one of the encapsulated bipyridinium (Table 1), in line with what reported for related pseudorotaxanes.[31] Moreover, upon increasing the scan rate another anodic peak appears at more positive potentials (not shown in Figure 5; see Figure S27, ESI), at a value close to that of the oxidation of the radical cation to the dication in the free axle. The second reduction process of **9** in CH_2Cl_2 is not affected by the scan rate. Its potential (-0.86 V, Table 1) is significantly less negative than that of the corresponding process in [1]rotaxane **11**, indicating that the bipyridinium radical cation of the lasso is no longer engulfed inside the calixarene (*vide supra*).

Table 1. Halfwave reduction potentials vs. SCE of compounds **9** – **11**

	CH_3CN		CH_2Cl_2	
	E_1 / V	E_2 / V	E_1 / V	E_2 / V
9	-0.60	-0.88	-0.65[a]	-0.86
10	-0.41	-0.87	-0.27	-0.82
11	-0.63	-1.18	-0.72	-1.20

[a] Peak potential value obtained from differential pulse voltammetry.

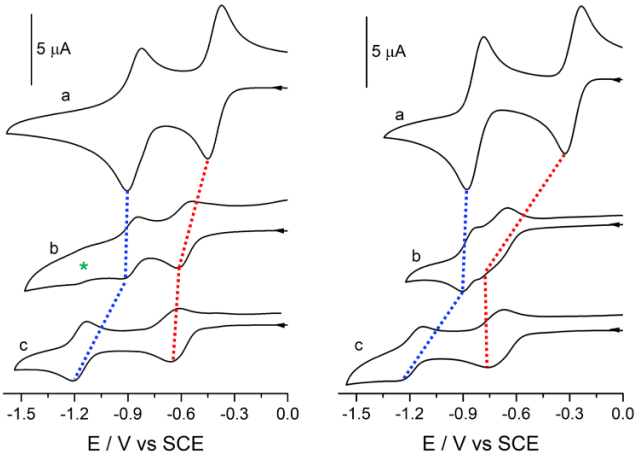

Figure 5 Cyclic voltammetric curves in CH_3CN (left) and CH_2Cl_2 (right) of thread **10** (a), [1]pseudorotaxane **9** (b) and [1]rotaxane **11** (c). Concentrations: **10**: 2.4×10^{-4} M in CH_3CN and 3.0×10^{-4} M in CH_2Cl_2; **9**: 1.5×10^{-4} M; **11**: 1.8×10^{-4} M. Scan rate 100 mV/s. The red and blue lines are a guide for the eye to facilitate the comparison between the potential values of the first and second reduction processes, respectively. The green asterisk marks a weak wave observed in CH_3CN at ca. -1.2 V; see the text for details.

This process, however, is also slightly more negative (40 mV) than the corresponding process in free axle **10**. Such a non-negligible difference would suggest that the calixarene still exerts some influence on the covalently linked bipyridinium radical cation arm, possibly mediated by the counteranion(s) bound at the urea units at the receptor upper rim. Effects of this kind are enhanced in the apolar, non-competitive CH_2Cl_2 with respect to CH_3CN.

Digital simulations of the CV curves were performed in order to gain some insight into the kinetics and thermodynamics of the threading and dethreading processes. The voltammetric curves were simulated with the mechanism reported in Scheme 2, by fixing the values of the reduction potentials of the free (E_1^f and E_2^f) and complexed (E_1^c and E_2^c) species to the ones of **10** and **11**, respectively. The results of the simulation were compared with the experimental data in CH_3CN for a selected scan rate (Figure S28, ESI). The association constant of the dicationic species is around 10^3, and the process is fast, with a rate constant k_1 larger than 5×10^4 s^{-1}, thus supporting the reversibility of the switching process. On the other hand, the threading/dethreading kinetics of the radical cation species are slow (k_2 around 1 s^{-1}, and k_{-2} around 5 s^{-1}), and these values account for the fact that part of the molecules is still encapsulated after the second reduction, as confirmed by the presence of a process at -1.2 V, marked with an asterisk in Figure 5 (*vide supra*). The experimental data do not allow remarks on the kinetics of the processes associated with the neutral species.

The simulation of the experiments performed in CH_2Cl_2 is less straightforward. The cyclic voltammetric curves of [1]pseudorotaxane **9** in CH_2Cl_2 cannot be reproduced by the simulation experiments if **10** and **11** are taken as model compounds for the free and encapsulated electroactive moiety, respectively. Indeed, the value of the second quasi-reversible reduction potential cannot be ascribed either to the free or to the encapsulated species.

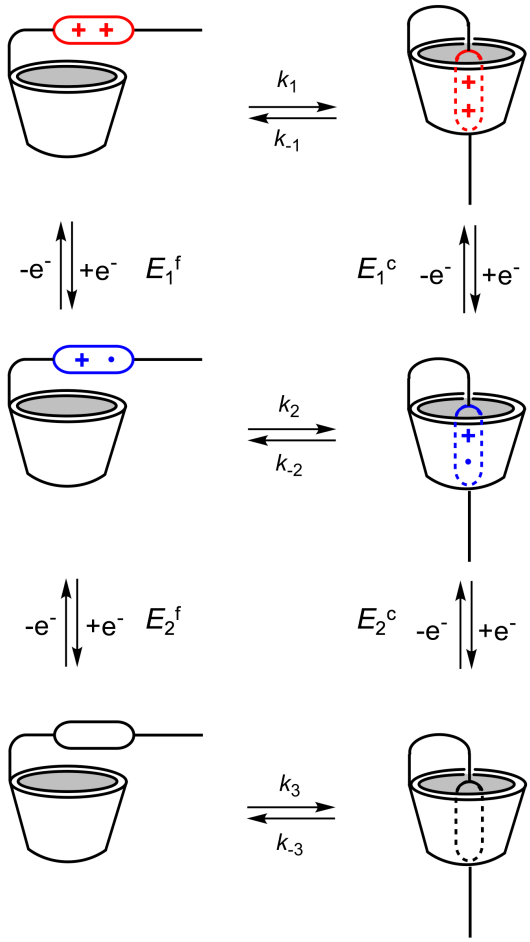

Scheme 2. Schematic representation of the threading/dethreading equilibria (horizontal processes) and the redox reactions (vertical processes) of [1]pseudorotaxane **9** in solution.

The large positive shift with respect to [1]rotaxane **11** would suggest that the radical cation is not encapsulated anymore inside the cavity of the calixarene; nevertheless, the small negative shift with respect to **10** would suggest that the monoreduced axle is still affected by the proximity of the wheel.

In the absence of an adequate model compound, only qualitative considerations can be made, based on the shape of the CV curves. In analogy with the results obtained in CH_3CN, a large association constant of the dicationic complex can be inferred. Based on the position and relative separation of the peaks of the first reduction wave, the complex should be even more stable than in CH_3CN, with an association constant larger than 10^4. On the other hand, the values of k_2 and k_{-2} (Scheme 2) can be related to two experimental observations: i) after the first reduction there is no residual signal of the encapsulated axle and ii) the anodic peak of the monoreduced axle splits into two signals on increasing the scan rate. The first observation implies faster kinetics for the monoreduced bipyridinium (k_2 and k_{-2}) with respect to the corresponding processes in CH_3CN. A qualitative simulation suggests that the value for k_2 and k_{-2} could be one or two orders of magnitude larger than in CH_3CN. The second observation would suggest that at relatively slow scan rates the equilibrium between free and complexed

monoreduced species (Scheme 2, second row) is fast enough and a quasi-reversible process is observed, whereas on increasing the scan rate some free monoreduced axle is present.

EPR measurements

EPR spectra of $\mathbf{9}^{+\bullet}$ and $\mathbf{11}^{+\bullet}$ were also recorded after electrochemical reduction of the corresponding diamagnetic precursors in deoxygenated CH_3CN or CH_2Cl_2 at room temperature. The spectral shape of $\mathbf{9}^{+\bullet}$ obtained in both solvents could be well reproduced by assuming a symmetric distribution of spin density on the two rings. As an example in Figure 6 is reported the EPR spectrum of $\mathbf{9}^{+\bullet}$ obtained in CH_3CN with the corresponding simulations calculated by assuming the coupling of the unpaired electron with two equivalent N atoms and three groups of four equivalent protons: one group is due to the methylene chains, and the other two equivalent sets arise from the aromatic protons groups. The values of hyperfine splitting constants employed in the theoretical simulation are reported in Table 2.

We have already shown that trapping $bpy^{+\bullet}$ in the asymmetric wheel of a calixarene, induces a non-symmetric distribution of the spin density in the two heterocyclic rings.[36] Thus, the symmetric distribution of the spin density on the two rings of the bipyridine radical cation found in $\mathbf{9}^{+\bullet}$ suggests that the radical unit is not interacting with the asymmetric cavity of the calixarene unit and that the addition of one electron on the bipyridinium site induces its displacement away from the wheel.

Table 2. EPR hyperfine splitting constants (a, in Gauss) of radical cations obtained after electrochemical reduction of the bipyridinium unit at room temperature.

	10 (CH_3CN)	**9** (CH_3CN)	**9** (CH_2Cl_2)	**11** (CH_3CN)
aN	4.11	4.11	4.11	4.34
aN	4.11	4.11	4.11	3.92
$a$$CH_2$	4.07	4.04	3.95	3.93
$a$$CH_2$	4.07	4.04	3.95	2.76
a(Ar)2H_β	1.59	1.64	1.63	1.84
a(Ar)2H_β	1.59	1.64	1.63	1.62
a(Ar)2H_α	1.10	1.10	1.08	1.33
a(Ar)2H_α	1.10	1.10	1.08	0.89

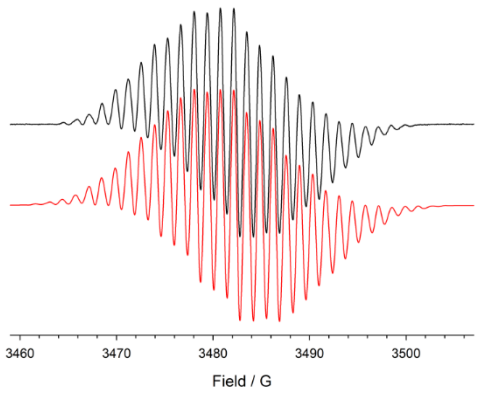

Figure 6 EPR spectrum of the radical cation $\mathbf{9}^{+\bullet}$ in acetonitrile (black) with the corresponding theoretical simulations (red).

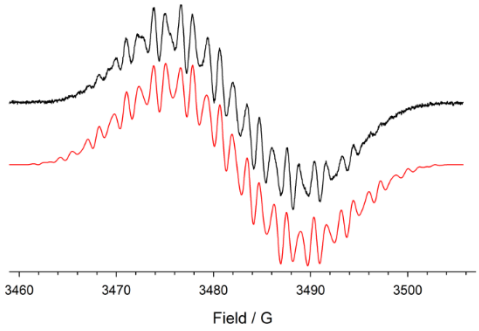

Figure 7 EPR spectrum (black) of the radical cation $\mathbf{11}^{+\bullet}$ in acetonitrile with the corresponding theoretical simulations (red).

This conclusion was further supported by recording the EPR spectrum of the [1]rotaxane **11** after electrochemical reduction in acetonitrile. The spectrum shape of $\mathbf{11}^{+\bullet}$ (Figure 7), clearly shows a non-symmetric distribution of the spin density in the two heterocyclic rings as expected for [1]rotaxane in which the mechanical bond forces $bpy^{+\bullet}$ radical to interact with the asymmetric calixarene cavity. The EPR fitting parameters are summarised in Table 2. The EPR spectrum of $\mathbf{11}^{+\bullet}$ was also recorded in CH_2Cl_2. In this case, however, a very broad, unresolved spectrum was obtained, and the determination of hyperfine splitting constants was not possible.

Conclusions

Important information about the reactivity of calixarene derivatives has been reported in this paper. New strategies for the synthesis of hetero-substituted tris(phenylureido) calix[6]arene have been optimised; these latter macrocycles, in some cases, have been further functionalised with viologen derivatives through a supramolecularly assisted reaction. A self-complexing molecule, able to modify its association properties depending on its concentration in apolar media, has been synthesised and characterized as the first example of a calix[6]arene-based [1]pseudorotaxane. Moreover, it has been demonstrated that this artificial molecular lasso can be switched between self-threaded and dethreaded structures by redox stimulation, with solvent-dependent thermodynamic and kinetic features. This prototype of a molecular machine paves the way for the construction of more sophisticated working devices in which appropriate external inputs may loosen or tighten the loop defined by the self-engulfed viologen bracket.[39] It has also been observed that this molecular design can form the basis for the construction of [*c*2]daisy chain architectures, which are unprecedented for calixarene macrocycles. Owing to the presence of the ω-hydroxy terminal substituent, the linear portion of the molecule can be endowed with a dumb stopper, as in the present case, or, in a perspective, with moieties – *e.g.*, recognition sites, ligands, etc. – that could generate more extended and functionally richer architectures. Performing research in this direction is critical to harness in full the currently underexploited peculiar features of calix[6]arene hosts for the construction of molecular-based devices and materials.

Experimental Section

All solvents were dried using standard procedures; all other reagents were of reagent grade quality obtained from commercial suppliers and were used without further purification. NMR spectra were recorded either at 300 or 400 MHz for ^{1}H and 100 MHz for ^{13}C. Chemical shifts are expressed in ppm (δ) using the residual solvent signal as internal reference (7.16 ppm for C_6H_6 and 7.26 ppm for $CHCl_3$). Mass spectra were recorded in ESI mode. All spectroscopic measurements were performed on air-equilibrated CH_3CN and CH_2Cl_2 (Uvasol) solutions at room temperature. Absorption spectra were recorded on a Cary300 (Agilent Technologies) spectrophotometer. Calix[6]arene **2**,[28] viologen axles **8**[30] and **10**,[31] and [2]rotaxane **12**[30] were synthesised according to published procedures. Molecular mechanics calculations were carried out using the MMFF94 force field[40] using the Avogadro software.[41] As observed by other authors,[42,43] the elemental analyses of calixarenes are very often incorrect. Nevertheless, the spectral data were in full agreement with the proposed structure of these new compounds (see ESI).

Synthesis

Methyl 2-(4-isocyanatophenyl)acetate (3). Under inert atmosphere, a solution of methyl (4-aminophenyl)acetate (1.0 g, 6.1 mmol) and triethylamine (0.6 g, 6.1 mmol) in dry dichloromethane (25 ml) was dropwise added to a solution of triphosgene (0.52 g, 2.1 mmol) in dry dichloromethane (10 ml), kept at 0° C through an external ice bath. The reaction mixture was stirred for 30 min at room temperature, and then the solvent was evaporated to dryness under reduced pressure. The sticky oily residue was extracted thrice with *n*-hexane (3×25 ml). The combined organic phases were evaporated to dryness under reduced pressure to give 0.64 g of **3** as a colourless oil (55%). ^{1}H NMR ($CDCl_3$, 400 MHz) δ= 7.26 (d, 2H, *J* = 8.0 Hz), 7.08 (d, 2H, *J* = 8.0 Hz), 3.72 (s, 2H), 3.63 (s, 2H); ^{13}C NMR ($CDCl_3$, 100 MHz) δ = 171.7, 132.4, 131.6, 130.5, 124.8, 52.2, 40.5; MS (ESI): m/z = 192.1 [100, M+H]. Elemental analysis calculated for $C_{10}H_9NO_3$: C, 62.82; H; 4.75; N, 7.33; found: 62.95; H, 4.91; N, 6.99.

Calix[6]arene (7). Under inert atmosphere, to a solution of **2** (0.15 g, 0.13 mmol) in dichloromethane (20 ml), a solution of isocyanates **3** (0.05 g, 0.26 mmol) and **4** (0.06 g, 0.54 mmol) in dichloromethane (10 ml) was dropwise added. The reaction mixture was stirred for two hours at room temperature. After this period, the solvent was evaporated to dryness under reduced pressure. Chromatographic purification of the solid residue (SiO_2, DCM:EtOAc = 85:15) afforded 0.08 g of **7** as a pale amorphous yellow solid (38%). ^{1}H NMR ($CDCl_3$, 400 MHz) δ = 7.4-6.6 (m, 26H), 6.0 (br. s, 6H), 4.4 (br. s, 6H), 3.9 (br. s, 6H), 3.7-3.6 (m, 11H), 3.5 (br. s, 6H), 2.9 (br. s, 9H), 1.3-0.9 (m, 27H); ^{13}C NMR (100 MHz) δ = 172.2, 154.6, 151.8, 146.7, 135.7, 133.0, 129.7, 128.9, 128.4, 127.8, 127.6, 122.6, 120.1, 72.4, 72.1, 69.9, 66.9, 60.3, 52.0, 40.5, 34.2, 31.5, 31.2, 31.0, 29.7, 15.3, 14.1; MS (ESI) m/z: 1538.8 [50, M+H], 1539.8 [30, M+H+1], 1560.8 [100, M+Na], 1561.8 [50, M+Na+1]. Elemental analysis calculated for $C_{93}H_{112}N_6O_{14}$: C, 72.63; H, 7.34; N, 5.46; found: 71.15; H, 6.85; N, 5.06.

Pseudorotaxane P[7⊃8]. To a solution of **7** (0.10 g, 0.07 mmol) in toluene (20 ml), axle **8** (0.05 g, 0.08 mmol) was added. The resulting heterogeneous mixture was stirred at room temperature for at least 2 hours during which it gradually turned homogeneous and deep red coloured. After this period, the solution was filtered to remove possible traces of undissolved salt **8**. The resulting filtered solution was evaporated under reduced pressure to afford pseudorotaxane P[**7**⊃**8**] as an amorphous red solid compound in quantitative yield. ^{1}H NMR ($CDCl_3$, 400 MHz) δ= 8.7-8.5 (m, 6H), 7.8-7.7 (m, 6H), 7.6-7.3 (m, 14H), 7.21 (d, 4H, *J* = 8.4 Hz), 7.1-6.6 (m, 16H), 6.1 (br. s, 2H), 4.52 (d, 6H, *J* = 14.8 Hz), 4.1-3.9 (m, 15H), 3.9-3.8 (m, 8H), 3.8-3.5 (m, 13H), 3.5-3.3 (m, 8H), 3.2 (br. s, 2H), 2.38 (s, 6H), 1.9 (br. s, 2H), 1.8 (br. s, 4H), 1.7 (br. s, 2H), 1.5-1.0 (m, 48H), 0.9-0.7 (m, 4H). ^{13}C NMR (100 MHz): δ= 153.2, 152.5, 148.0, 144.2, 142.8, 141.9, 140.1, 136.5, 133.8, 131.9, 129.6, 128.9, 128.8, 128.7, 126.7, 126.1, 125.2, 124.2, 121.4, 117.7, 116.6, 77.3, 77.2, 77.0, 76.7, 72.3, 70.1, 66.6, 62.6, 62.3, 61.4, 52.0, 40.1, 34.5, 33.3, 31.9, 31.4, 29.7, 29.1, 25.5, 22.7, 21.4, 15.3, 14.1. MS (ESI) m/z: 948.2 $[M\text{-}2TsO]^{2+}$. Elemental analysis calculated for $C_{129}H_{160}N_8O_{22}S_2$: C, 69.21; H, 7.20; N, 5.01; S, 2.86; found: 67.94; H, 7.61; N, 4.72; S, 2.25.

[1]pseudorotaxane (9). To a solution of pseudorotaxane P[**7**⊃**8**] (0.15 g, 0.07 mmol) in refluxing toluene (20 ml), *p*-toluenesulfonic acid monohydrate (0.002 g, 0.01 mmol) was added. The resulting homogeneous solution was refluxed for two hours. After this period, the solvent was evaporated to dryness under reduced pressure. Chromatographic purification (SiO_2, DCM:MeOH = 95:5) of the resulting residue yielded 0.1 g of **9** as a red solid compound (65%). ^{1}H NMR ($CDCl_3$, 400 MHz) δ= 8.7-8.5 (m, 6H), 7.9 (br. s, 2H), 7.82 (d, 4H, *J* = 8.0 Hz), 7.6-7.3 (m, 12H), 7.2-6.6 (m, 16H), 7.20 (d, 4H, *J* = 8.0 Hz), 7.2-7.0 (m, 8H), 7.0-6.4 (m, 9H), 5.9 (br. s, 2H), 4.6-4.3 (m, 6H), 4.1-3.7 (m, 21H), 3.7-3.5 (m, 6H), 3.5-3.3 (m, 8H), 3.1 (br. s, 2H), 2.38 (s, 6H), 2.1 (br. s, 2H), 1.8 (br. s, 4H), 1.7 (br. s, 2H), 1.5-1.0 (m, 48H), 1.0-0.7 (m, 6H). ^{13}C NMR (100 MHz): δ= 171.6, 153.0, 152.1, 148.1, 144.3, 142.7, 142.1, 140.2, 140.0, 139.2, 139.1, 136.7, 134.3, 131.8, 129.8, 129.7, 129.1, 128.8, 127.8, 127.6, 126.1, 125.4, 124.1, 121.5, 117.7, 116.8, 116.6, 77.3, 77.2, 77.0, 76.7, 70.1, 66.6, 62.5, 61.4, 41.7, 34.5, 34.3, 31.3, 29.7, 29.3, 22.7, 21.5, 21.4, 15.3, 14.1.; MS (ESI) m/z = 932.2 [100, M-2TsO] (z = 2). Elemental analysis calculated for $C_{128}H_{156}N_8O_{21}S_2$: C, 69.67; H, 7.13; N, 5.08; S, 2.91; found: 68.21; H, 7.14; N, 4.86; S, 2.50.

[1]rotaxane (11). To a solution of **9** (0.05 g, 0.02 mmol) in toluene (0.6 ml), diphenylacetyl chloride (0.008 g, 0.04 mmol) and triethylamine (0.008 g, 0.04 mmol) were added. The resulting homogeneous solution was stirred overnight. Afterwards, the solvent was evaporated under reduced pressure and the solid residue was purified by column chromatography (SiO_2, DCM:MeOH = 97:3) to afford 0.025 g of **11** as an amorphous red solid compound (52%). ^{1}H NMR ($CDCl_3$, 400 MHz) δ= 9.0-8.5 (m, 6H), 7.9 (br. s, 2H), 7.84 (d, 4H, *J* = 8.0

Hz), 7.6-7.3 (m, 24H), 7.3-7.2 (m, 6H), 7.2-7.0 (m, 8H), 7.0-6.7 (m, 6H), 6.6 (br. s, 2H), 5.9 (br. s, 2H), 5.07 (s, 1H), 4.6-4.4 (m, 6H), 4.35 (t, 2H, *J* = 6.8 Hz), 4.3-4.0 (m, 6H), 4.0-3.9 (m, 11H), 3.8 (br. s, 6H), 3.7-3.5 (m, 6H), 3.5-3.3 (m, 8H), 3.2 (br. s, 2H), 2.38 (s, 6H), 2.1 (br. s, 2H), 1.9 (br. s, 2H), 1.8 (br. s, 2H), 1.7 (br. s, 4H), 1.5-1.0 (m, 50H), 0.8-0.4 (m, 6H). ^{13}C NMR (100 MHz): δ= 172.5, 171.6, 152.9, 152.5, 148.1, 144.3, 142.8, 142.2, 140.3, 140.0, 138.6, 136.7, 133.8, 133.6, 131.9, 131.8, 129.7, 129.1, 128.8, 128.7, 128.6, 128.6, 128.5, 128.1, 127.8, 127.6, 127.4, 126.1, 125.4, 124.0, 121.5, 117.7, 116.8, 116.6, 77.2, 72.7, 72.4, 70.0, 66.6, 65.0, 63.4, 61.3, 60.4, 57.1, 41.7, 34.5, 34.3, 31.9, 31.3, 29.7, 29.7, 29.5, 29.4, 29.2, 28.5, 27.7, 26.0, 24.8, 22.7, 21.4, 15.4, 14.1. HR-MS (ESI, Orbitrap LQ) calculated for $C_{128}H_{152}N_8O_{16}$ m/z (z = 2): 1028.56577 (72), 1029.06744 (100), 1029.56912 (68), 1030.07080 (31), 1030.57248 (11), 1031.07415 (3). Elemental analysis calculated for $C_{142}H_{166}N_8O_{22}S_2$: C, 71.03; H, 6.97; N, 4.67; S, 2.67; found: 70.86; H, 7.17; N, 4.38, S, 2.31.

NMR Diffusion measurements

DOSY experiments were carried out in $CDCl_3$ at 300 K either on a Bruker Avance 300 or Avance 400 Spectrometer using a stimulated echo sequence with bipolar gradients (STEbp). The mean diffusion coefficient *D* of the species present in solution was determined by using the Bayesian analysis implemented in the MestReNova software. For each sample, 16 experiments were carried out, in which the gradient strength *g* was varied from 5 to 95% of the maximum gradient intensity (5.35 G/mm).

Electrochemical measurements

Cyclic voltammetry (CV) and differential pulse voltammetry (DPV) experiments were performed in argon-purged dry CH_3CN or CH_2Cl_2 (Sigma-Aldrich), in the presence of a 100-fold excess of tetrabutylammonium hexafluorophosphate ($TBAPF_6$) as supporting electrolyte, using an Autolab 30 multipurpose potentiostat, interfaced to a PC. A glassy carbon electrode (Amel, diameter 3 mm), carefully polished with an alumina-water slurry on a felt surface immediately before use, was used as working electrode. A Pt wire, separated from the solution by a frit, was employed as the counterelectrode, whereas an Ag wire was used as a quasi-reference electrode. Ferrocene was added as an internal standard. Cyclic voltammograms were recorded at sweep rates varying from 0.05 to 5 V s^{-1}. Differential pulse voltammograms were recorded with a rate of 0.02 V s^{-1}, with a peak height of 0.075 V and a peak width of 0.040 s. The IR compensation, implemented within the software, was employed to minimise the resistance of the solution. In any case, the full electrochemical reversibility of the voltammetric wave of ferrocene was taken as an indicator of the absence of uncompensated resistance effects.

EPR measurements

EPR spectra were recorded at room temperature using an ELEXYS E500 spectrometer equipped with an NMR gaussmeter for the calibration of the magnetic field and a frequency counter for the determination of *g*-factors that were corrected against that of the perylene radical cation in concentrated sulfuric acid (g = 2.002583). The electrochemical cell was homemade and consisted of an EPR flat cell (Wilmad WG-810) equipped with a 25×5×0.2 mm platinum gauze (cathode), and a platinum wire (anode).[44] The current was supplied and controlled by an AMEL 2051 general-purpose potentiostat. In a typical experiment, the cell was filled with an acetonitrile or dichloromethane solution of the appropriate substrate (ca. 1 mM) containing tetrabutylammonium hexafluorophosphate (ca. 0.1 M) as supporting electrolyte. After thoroughly purging the solution with N_2, spectra were recorded at different potential settings in the range 0 to –0.8 V. An iterative least-squares fitting procedure based on the systematic application of the Monte Carlo method was performed to obtain the experimental spectral parameters of the radical species.[45]

Acknowledgements

The authors thank Centro Interdipartimentale di Misure of the University of Parma for NMR and MS measurements and Paola Franchi for technical assistance in recording EPR spectra. This work was supported by the Italian MIUR (PRIN 20173L7W8K and FARE grant no. R16S9XXKX3), the Universities of Bologna and Parma, and it has been carried out within the COMP-HUB Initiative funded by the 'Departments of Excellence' program of the Italian Ministry for Education, University and Research (MIUR, 2018-2022).

Notes and references

‡ A further DOSY experiment was carried out by using the calix[6]arene-based [2]rotaxane **12** (see Chart 1) as the reference for the molecular weight determination. The results of such measurement are not directly comparable with those obtained with pseudorotaxane P[**1**⊃**10**], because the presence of the bulky stoppers on the thread changes significantly the shape of the rotaxane diffusing in the solution. Nonetheless, this experiment allowed us to exclude that the diffusion coefficient measured for the reference compound is affected by exchange phenomena with the solution since the thread is confined inside the wheel. The experiment yielded a significative higher value of *D* for the [2]rotaxane **12** to the one measured for **9** (see Figure S21, ESI), thus indirectly supporting the hypothesised [*c*2]daisy chain structure of the latter compound in solution.

1 V. Balzani, A. Credi and M. Venturi, *Molecular Devices and Machines: Concepts and Perspectives for the Nanoworld*: Second Edition, Wiley-VCH, Weinheim, 2008.
2 C. J. Bruns and J. F. Stoddart, *The Nature of the Mechanical Bond: From Molecules to Machines*, John Wiley & Sons, 2016.
3 M. Baroncini, L. Casimiro, C. de Vet, J. Groppi, S. Silvi and A. Credi, *ChemistryOpen*, 2018, **7**, 169–179.
4 B. A. Grzybowski and W. T. S. Huck, *Nat. Nanotechnol.*, 2016, **11**, 585–592.
5 J. D. Hegemann, M. Zimmermann, X. Xie and M. A. Marahiel, *Acc. Chem. Res.*, 2015, **48**, 1909–1919.
6 H. E. Elashal, R. D. Cohen, H. E. Elashal, C. Zong, A. J. Link and M. Raj, *Angew. Chem. Int. Ed.*, 2018, **57**, 6150–6154.
7 C. Zong, M. J. Wu, J. Z. Qin and A. J. Link, *J. Am. Chem. Soc.*, 2017, **139**, 10403–10409.

8 C. D. Allen and A. J. Link, *J. Am. Chem. Soc.*, 2016, **138**, 14214–14217.
9 C. Clavel, C. Romuald, E. Brabet and F. Coutrot, *Chem. Eur. J.*, 2013, **19**, 2982–2989.
10 Q. Zhou, P. Wei, Y. Zhang, Y. Yu and X. Yan, *Org. Lett.*, 2013, **15**, 5350–5353.
11 H. V. Schröder, J. M. Wollschläger and C. A. Schalley, *Chem. Commun.*, 2017, **53**, 9218–9221.
12 Y. Liu, A. H. Flood, R. M. Moskowitz and J. F. Stoddart, *Chem. Eur. J.*, 2005, **11**, 369–385.
13 T. Rama, A. Blanco-Gómez, I. Neira, O. Domarco, M. D. García, J. M. Quintela and C. Peinador, *Chem. Eur. J.*, 2017, **23**, 16743–16747.
14 Y. Wang, J. Sun, Z. Liu, M. S. Nassar, Y. Y. Botros and J. F. Stoddart, *Chem. Sci.*, 2017, **8**, 2562–2568.
15 Y. Liu, C. Chipot, X. Shao and W. Cai, *J. Phys. Chem. C*, 2014, **118**, 19380–19386.
16 J. Cao, X. Ma, M. Min, T. Cao, S. Wu and H. Tian, *Chem. Commun.*, 2014, **50**, 3224–3226.
17 A. Miyawaki, P. Kuad, Y. Takashima, H. Yamaguchi and A. Harada, *J. Am. Chem. Soc.*, 2008, **130**, 17062–17069.
18 B. Xia and M. Xue, *Chem. Commun.*, 2014, **50**, 1021–1023.
19 Y. Wang, J.-F. Xu, Y.-Z. Chen, L.-Y. Niu, L.-Z. Wu, C.-H. Tung and Q.-Z. Yang, *Chem. Commun.*, 2014, **50**, 7001–7003.
20 Q. Zhao, Y. Chen, B. Sun, C. Qian, M. Cheng, J. Jiang, C. Lin and L. Wang, *Eur. J. Org. Chem.*, 2019, **2019**, 3396–3400.
21 X.-S. Du, C.-Y. Wang, Q. Jia, R. Deng, H.-S. Tian, H.-Y. Zhang, K. Meguellati and Y.-W. Yang, *Chem. Commun.*, 2017, **53**, 5326–5329.
22 *Calixarenes and beyond*, eds. P. Neri, J. L. Sessler, M.-X. Wang, P. Neri, J. L. Sessler and M.-X. Wang, Eds., Springer International Publishing, 2016.
23 A. Arduini, G. Orlandini, A. Secchi, A. Credi, S. Silvi and M. Venturi, in *Reference Module in Chemistry, Molecular Sciences and Chemical Engineering*, Elsevier, 2014, pp. 1–26.
24 A. Arduini, G. Orlandini, A. Secchi, A. Credi, S. Silvi and M. Venturi, in *Calixarenes and Beyond*, eds. P. Neri, J. L. Sessler and M.-X. Wang, Springer International Publishing, Cham, 2016, pp. 761–781.
25 J. Rotzler, S. Drayss, O. Hampe, D. Häussinger and M. Mayor, *Chem. Eur. J.*, 2013, **19**, 2089–2101.
26 J.-N. Rebilly, A. Hessani, B. Colasson and O. Reinaud, *Org. Biomol. Chem.*, 2014, **12**, 7780–7785.
27 N. L. Strutt, H. Zhang, M. A. Giesener, J. Lei and J. F. Stoddart, *Chem. Commun.*, 2012, **48**, 1647–1649.
28 J. J. González, R. Ferdani, E. Albertini, J. M. Blasco, A. Arduini, A. Pochini, P. Prados and J. De Mendoza, *Chem. Eur. J.*, 2000, **6**, 73–80.
29 A. Arduini, F. Calzavacca, A. Pochini and A. Secchi, *Chem. Eur. J.*, 2003, **9**, 793–799.
30 A. Arduini, R. Bussolati, A. Credi, A. Pochini, A. Secchi, S. Silvi and Margherita. Venturi, *Tetrahedron*, 2008, **64**, 8279–8286.
31 A. Credi, S. Dumas, S. Silvi, M. Venturi, A. Arduini, A. Pochini and A. Secchi, *J. Org. Chem.*, 2004, **69**, 5881–5887.
32 A. Arduini, R. Ferdani, A. Pochini, A. Secchi and F. Ugozzoli, *Angew. Chem. Int. Ed.*, 2000, **39**, 3453–3456.
33 A. Arduini, F. Ciesa, M. Fragassi, A. Pochini and A. Secchi, *Angew. Chem. Int. Ed.*, 2005, **44**, 278–281.
34 Y. Cohen, L. Avram and L. Frish, *Angew. Chem. Int. Ed.*, 2005, **44**, 520–554.
35 Y. Cohen, L. Avram, T. Evan-Salem, S. Slovak, N. Shemesh and L. Frish, in *Analytical Methods in Supramolecular Chemistry*, ed. C. A. Shalley, John Wiley & Sons, Ltd, 2012, pp. 197–285.
36 V. Zanichelli, M. Bazzoni, A. Arduini, P. Franchi, M. Lucarini, G. Ragazzon, A. Secchi and S. Silvi, *Chem. Eur. J.*, 2018, **24**, 12370–12382.
37 V. Zanichelli, G. Ragazzon, A. Arduini, A. Credi, P. Franchi, G. Orlandini, M. Venturi, M. Lucarini, A. Secchi and S. Silvi, *Eur. J. Org. Chem.*, 2016, **2016**, 1033–1042.
38 R. Ballardini, A. Credi, M. T. T. Gandolfi, C. Giansante, G. Marconi, S. Silvi and M. Venturi, *Inorganica Chim. Acta*, 2007, **360**, 1072–1082.
39 C. Romuald, A. Ardá, C. Clavel, J. Jiménez-Barbero and F. Coutrot, *Chem. Sci.*, 2012, **3**, 1851–1857.
40 T. A. Halgren, *J. Comput. Chem.*, 1996, **17**, 616–641.
41 M. D. Hanwell, D. E. Curtis, D. C. Lonie, T. Vandermeerschd, E. Zurek and G. R. Hutchison, *J. Cheminformatics*, 2012, **4**, 17.
42 V. Böhmer, K. Jung, M. Schon, A. Wolff, *J. Org. Chem.*, 1992, **57**, 790-792.
43 C. D. Gutsche, K. A. See, *J. Org. Chem.* 1992, **57**, 4527-4539.
44 C. Boga, M. Calvaresi, P. Franchi, M. Lucarini, S. Fazzini, D. Spinelli and D. Tonelli, *Org. Biomol. Chem.*, 2012, **10**, 7986–7995.
45 P. Franchi, E. Mezzina and M. Lucarini, *J. Am. Chem. Soc.*, 2014, **136**, 1250–1252.